



HAL
open science

Analysis of the pressure effect on the crystallization kinetics of polypropylene: Dilatometric measurements and thermal gradient modeling

R. Fulchiron, E. Koscher, G. Poutot, D. Delaunay, G. Regnier

► To cite this version:

R. Fulchiron, E. Koscher, G. Poutot, D. Delaunay, G. Regnier. Analysis of the pressure effect on the crystallization kinetics of polypropylene: Dilatometric measurements and thermal gradient modeling. *Journal of Macromolecular Science Part B Physics*, 2007, 40 (3-4), pp.297-314. 10.1081/MB-100106159 . hal-02337605v1

HAL Id: hal-02337605

<https://hal.science/hal-02337605v1>

Submitted on 14 Dec 2022 (v1), last revised 3 May 2024 (v2)

HAL is a multi-disciplinary open access archive for the deposit and dissemination of scientific research documents, whether they are published or not. The documents may come from teaching and research institutions in France or abroad, or from public or private research centers.

L'archive ouverte pluridisciplinaire **HAL**, est destinée au dépôt et à la diffusion de documents scientifiques de niveau recherche, publiés ou non, émanant des établissements d'enseignement et de recherche français ou étrangers, des laboratoires publics ou privés.

**ANALYSIS OF THE PRESSURE EFFECT ON THE CRYSTALLIZATION KINETICS:
DILATOMETRIC MEASUREMENTS AND THERMAL GRADIENT MODELING.**

R. Fulchiron*, E. Koscher

Laboratoire des Matériaux Polymères et des Biomatériaux (UMR-CNRS 5627)

UCBL, Bât ISTIL, 43 Bd du 11 novembre 1918, 69622 Villeurbanne Cedex (France).

E-mail: fulchiro@matplast.univ-lyon1.fr.

G. Poutot, D. Delaunay

Laboratoire de Thermocinétique, Ecole Polytechnique de l'Université de Nantes (France)

G. Régnier

Laboratoire de Transformation et Vieillessement des Polymères - ENSAM Paris (France)

* To whom correspondence should be addressed

ABSTRACT

Dilatometric measurements in isobaric cooling mode are performed to study the pressure effects on the crystallization kinetics of polypropylene up to 100 MPa. The rough experimental specific volume curves are analyzed by taking into account the thermal gradient which appears in the sample even for relatively low cooling rates. The Tait equation is used to describe the specific volume of the purely amorphous phase and linear variations of the purely crystalline phase specific volume are considered. The relative crystallinity is modeled using the Nakamura equation which is relevant for non constant cooling rates. Considering an Avrami exponent of 3, the Nakamura rate constant is obtained first at atmospheric pressure and then generalized for higher pressures considering the equilibrium melting temperature variation. The obtained intrinsic specific volume is validated by computing the thermal gradient in the sample and comparing the calculated average specific volume to the experimental one.

KEYWORDS

Polypropylene, Pressure-Volume-Temperature Measurement, Thermal Modeling, Crystallization kinetics, Nakamura equation.

INTRODUCTION

The Pressure-Volume-Temperature (PVT) behavior is an important characteristic of thermoplastic polymers either for fundamental aspects (thermodynamics) or for practical applications (injection molding for example). Moreover when studying the polymer crystallization, one classical procedure to assess the kinetics of the transition is to investigate the influence of the cooling rate on the transition temperature. In that case, because of the poor thermal conductivity of the polymers, one must take care of the temperature gradient in the sample. When using a DSC, for example, the sample is so small that the temperature is reasonably considered homogeneous. Nevertheless, for pressure studies by dilatometry, the sample must be large enough (typically 1 cm³) to obtain an accurate measurement of the volume change. In that case, when the cooling rate increases, the thermal gradient in the sample must be considered, especially in the vicinity of the phase change where the enthalpy of crystallization can affect the temperature field. For these reasons the PVT measurements are generally achieved in isothermal or very low cooling rates conditions¹⁻³. The objective of this study is to establish a methodology in order to obtain reliable PVT diagrams for semi-crystalline polymers. Particularly, the thermal gradient effect in the experimental results is extracted in order to obtain the specific volume of the polymer independently of the sample size. The present study follows and completes a previous one where the thermal aspect was already described⁴. In this work, the specific volume evolution, and especially the cooling rate and the pressure effects on the crystallization kinetics are thoroughly analyzed.

EXPERIMENTAL

In this work, the studied polymer was a injection grade of isotactic polypropylene (*i*-PP) supplied by Solvay (Brussels, Belgium) with the commercial name Eltex HV252. The Melt Flow Index of

this polypropylene was $MFI_{2/230}=11\text{g}/10\text{min}$.

The PVT experimental results were obtained using a piston type dilatometer (*PVT100*) commercialized by SWO Polymertechnik GmbH (Krefeld, Germany). The detailed description of the system was given elsewhere⁴ hence, only the main characteristics are recalled in this paper. The diameter of the cylindrical cell is 7.7 mm and the length of the sample is typically around 15 mm. The temperature is controlled using a thermocouple located very close to the periphery of the sample, in the middle of its height. The pressure on the sample is ensured by a lower fixed piston and an upper mobile one. In order to avoid polymer leakage, PTFE seals are placed between the sample and the pistons. From the length of the sample, measured by a displacement sensor, the specific volume is obtained. Experiments were performed in isobaric cooling mode for different pressures ranged between 20 and 100 MPa and different cooling rates ranged between 1°C/min and 35°C/min.

At atmospheric pressure, crystallization experiments were carried out using a DSC7 from Perkin-Elmer (Norwalk, Connecticut) calibrated with indium and zinc. The procedure for isothermal crystallization experiments was as follows: The sample of about 10 mg was molten at 210°C during five minutes. Then, it was first rapidly cooled down to a temperature of ten Celsius degrees higher than the chosen crystallization temperature T_c . Second, it was cooled down to T_c using a cooling rate of 10°C/min. This procedure allowed us to prevent an undershoot below T_c . The crystallization temperatures were ranged between 124°C and 140°C. For constant cooling rate crystallization experiments, the sample was also molten at 210 °C during five minutes and cooled with the chosen cooling rate ranged between 1 and 40 °C/min. Heating runs at 10°C/min were then performed on the same samples to determine their crystallinity and its evolution with the previous cooling rate. Measured enthalpies of melting ΔH were compared to the enthalpy of fusion of the infinite crystal⁵ $\Delta H_\infty = 148\text{ J/g}$. Furthermore, the crystallinity of samples crystallized at 1°C/min at different pressures in the PVT analyzer were also determined from DSC melting experiments.

RESULTS AND DISCUSSION

Thermal Modeling

The thermal modeling of the PVT sample was achieved following a procedure previously described⁴. Considering that the problem is axisymmetric and that there is no heat flux through the pistons thanks to the PTFE seals, the heat equation for a radius r and a time t is expressed by:

$$\frac{C_p}{V_{sp}} \frac{\partial T}{\partial t} - \frac{\lambda}{r} \frac{\partial T}{\partial r} = \frac{\partial}{\partial r} \left(\lambda \frac{\partial T}{\partial r} \right) + \frac{X_\infty \Delta H_\infty}{V_{sp}} \frac{\partial \alpha}{\partial t} \quad (1)$$

where C_p is the heat capacity, λ is the thermal conductivity, V_{sp} is the specific volume, α is the relative crystallinity, X_∞ is the final crystallinity and T is the temperature.

Obviously, all the parameters which appear in eq. (1) can be temperature, pressure and even time dependent. These parameters will be detailed in the next section. A Crank-Nicholson finite difference scheme was used to solve the thermal problem with the following bounding conditions. At time equal to zero, the temperature is homogeneous in the sample. For each time, the temperature gradient is null in the axis and the peripheral temperature is given by the control temperature.

Heat Capacity and Thermal Conductivity

Following previous results^{4,6}, the heat capacity and the thermal conductivity were described using simple mixing rules between the solid state and the liquid state values weighted by the relative crystallinity:

$$C_p = \alpha C_{ps} + (1 - \alpha) C_{pa} \quad (2)$$

where C_{ps} and C_{pa} are the heat capacity of the solid state and the liquid state respectively.

$$\lambda = \alpha \lambda_s + (1 - \alpha) \lambda_a \quad (3)$$

where λ_s and λ_a are the thermal conductivity of the solid state and the liquid state respectively.

It must be pointed out that a simple mixing rule is not rigorously appropriate for the thermal conductivity (eq. 3) because it is not an additive property. Nevertheless, this approximation was reasonably considered adequate for our purpose because it can introduce only a small error in the crystallization temperature domain which is relatively narrow as it will be shown further.

Moreover, linear temperature dependences for C_{ps} , C_{pa} , λ_s and λ_a were obtained leading to:

$$C_{ps}(\text{J/kgK}) = 10,68T(^{\circ}\text{C}) + 1451 \quad (4)$$

$$C_{pa}(\text{J/kgK}) = 3,10T(^{\circ}\text{C}) + 2124 \quad (5)$$

$$\lambda_s(\text{W/mK}) = -4,96.10^{-4}T(^{\circ}\text{C}) + 0,31 \quad (6)$$

$$\lambda_a(\text{W/mK}) = -6,25.10^{-5}T(^{\circ}\text{C}) + 0,189 \quad (7)$$

Besides, a pressure dependence could also be considered but, because of a lack of experimental results, this pressure dependence was not introduced in our analysis. Nevertheless, as it will be shown further in this article, a pressure dependence as well as a cooling rate dependence of the relative crystallinity α were taken into account. Consequently, the change of the transition temperature domain with the pressure and the cooling rate appears in the C_p and λ values.

Specific Volume

The specific volume (V_{sp}) evolution with the temperature was described considering a blending law of the amorphous (or liquid) phase and the crystalline phase specific volumes (respectively V_a and V_c). The balance between each phase is given by the mass crystallinity equal to the product αX_{∞} .

$$V_{sp} = \alpha X_{\infty} V_c + (1 - \alpha X_{\infty}) V_a \quad (8)$$

First, the amorphous phase specific volume V_a was described using the well known empirical Tait equation:^{3,7}

$$V_a = V_0(T) \left[1 - C \ln \left(1 + \frac{P}{B(T)} \right) \right] \quad (9)$$

where C is considered as a universal constant equal to 0.0894.

The functions $V_0(T)$ and $B(T)$ can be described by linear, second order polynomial or, more currently, by exponential expressions. In this work, exponential expressions were used. The parameters of the Tait equation were fitted on the liquid part of experimental PVT data obtained in isobaric cooling mode with a low cooling rate (1°C/min) to avoid the thermal gradient effect. The results of the fitting were:

$$V_0(T) = 1.1546 \exp\left(6.74 \times 10^{-4} T\right) \text{ (cm}^3/\text{g)} \quad (10)$$

$$B(T) = 148.69 \exp\left(-4.3767 \times 10^{-3} T\right) \text{ (MPa)} \quad (11)$$

where T is in °C.

It can be pointed out that eq.10 and eq.11 are similar to those given by Rodgers⁷. As shown in Figure 1, the calculated curves are very close to the experimental specific volume in the liquid part. Moreover, the specific volume of the purely amorphous phase, calculated at atmospheric pressure and ambient temperature is consistent with literature data⁸ (see Figure 1).

As concerns the solid part of the PVT diagrams (eq.8 with $\alpha=1$), the description appeared incorrect by assuming no variation of the purely crystalline specific volume V_c with P and T . Indeed, as shown in Figure 2, considering a constant V_c , the slopes of the calculated curves is much lower than the experimental ones and the shift between each pressure is not large enough. In that case, the change of the calculated specific volume is only due to the amorphous contribution given by the Tait equation. Moreover, this description remains inaccurate whatever the used final crystallinity (X_∞) in a reasonable range. Therefore, despite no explicit establishment in the literature, linear variations of V_c with the pressure and the temperature were assumed to describe the solid state of the specific volume. The parameters of these variations were determined using the solid part of a low cooling rate (1°C/min) PVT diagram to avoid thermal gradient effects. Moreover, it was imposed that the calculated value of V_c at ambient temperature and atmospheric pressure was consistent with literature data given for the density of the α crystalline form⁹ ($\rho_c=0.936 \text{ g/cm}^3$). It must be added that for this calculation, X_∞ was considered independent of the pressure and adjusted

together with the parameters. Following these criterions, the best fit was obtained with $X_{\infty}=0.684$ leading to:

$$V_c(P,T) = 1.0632 + 2.071 \times 10^{-4} T - 1.901 \times 10^{-4} P \quad (12)$$

where T is in °C, P is in MPa and V_c is in cm³/g.

As shown in Figure 2, the solid part of the experimental PVT diagram is correctly described by eq.8 (with $\alpha=1$ and $X_{\infty}=0.684$) and eq.12. Moreover, the calculated value of X_{∞} is consistent with the experimental results obtained for samples crystallized at different pressures with a cooling rate of 1°C/min (Table 1). Indeed, for a crystallization pressure varying from 0.1 MPa to 100 MPa, only a slight decrease of the crystallinity is observed from 0.677 to 0.623.

Relative Crystallinity

The crystallization kinetics was analyzed on the basis of the Nakamura equation¹⁰⁻¹¹ which is expressed by:

$$\alpha = 1 - \exp \left[- \left(\int_0^t K(T) d\tau \right)^n \right] \quad (13)$$

where $K(T)$ is the Nakamura rate constant and n is the Avrami exponent. The main advantage of this expression is its ability to describe the relative crystallinity for a non-constant cooling rate which is the case inside the PVT sample. First, the determination of the rate constant $K(T)$ was achieved at atmospheric pressure from isothermal and constant cooling rate crystallization DSC experiments. Indeed, the DSC crystallization results were analyzed using the Avrami¹²⁻¹⁴ (eq.14) and the Ozawa¹⁵ (eq.15) expressions for isothermal and constant cooling rate experiments respectively:

$$\alpha(t) = 1 - \exp \left(- k(T) t^n \right) \quad (14)$$

where k is the Avrami rate constant.

$$\alpha(T) = 1 - \exp\left(-\frac{\kappa(T)}{\phi^n}\right) \quad (15)$$

where κ is the Ozawa rate constant and ϕ is the cooling rate.

Moreover, the Nakamura rate constant is mathematically linked to the Avrami and Ozawa rate constants¹⁶⁻¹⁷:

$$K = k^{1/n} = -\frac{d\left(\kappa^{1/n}\right)}{dT} \quad (16)$$

Although the Avrami exponent n could have been an outcome of the analysis, it was fixed to $n=3$ in our work because this value is frequently encountered in the literature for *i*-PP¹⁷⁻²⁰ which commonly exhibits a heterogeneous nucleation process.

From isothermal crystallization DSC experiments, the relative crystallinity function $\alpha(t)$ was obtained by the ratio of the crystallization peak area before time t over its total area. Then, for each experimental temperature, the Avrami rate constant $k(T)$ was deduced from eq.14 with $n=3$.

For constant cooling rates experiments, the relative crystallinity function $\alpha(T)$ was calculated for every cooling rate by dividing the crystallization peak area above the temperature T by its total area. Then, the Ozawa rate constant $\kappa(T)$ was calculated by fitting eq.15 with $n=3$ on the whole collection of relative crystallinity curves considering a polynomial evolution of $\ln(\kappa(T))$.

Knowing $k(T)$ and $\kappa(T)$, the Nakamura rate constant $K(T)$ was then obtained from eq.16. The results are plotted in Figure 3 showing the agreement between data deduced from isothermal and non isothermal experiments in the overlapping domain. Then, $K(T)$ was described by the following equation:

$$\ln(K(T)) = -18.38 + 0.3763T - 2.19 \times 10^{-3} T^2 \quad (17)$$

with T in °C and $K(T)$ in s⁻¹.

Moreover, the suitability of eq.13 and eq.17 is shown in Figure 4 where the calculated relative crystallinity curves are very close to the experimental ones for cooling rates ranged between 1 and 40°C/min.

Furthermore, the pressure effect on the crystallization kinetics was evaluated by considering first the temperature of the crystallization onset (T_c) for low cooling rate experiments (2°C/min) and different pressures. The crystallization temperature versus the pressure is shown in Figure 5. Then, it was described by a second order polynomial:

$$T_c = T_c^{Patm} + 0.283 P - 2.08 \times 10^{-4} P^2 \quad (18)$$

where T_c is in °C and P is in MPa.

In order to generalize the pressure effect for any cooling rate, it was considered that the crystallization kinetics is mainly driven by the supercooling²¹⁻²² which is the difference between the equilibrium melting temperature and the actual temperature ($\Delta T = T_m^0 - T$). In other words, for a given cooling rate the crystallization occurs at the same supercooling whatever the pressure.

Therefore, the previous polynomial which describes the crystallization temperature (eq.18) directly reflects the variation of the equilibrium melting temperature with the pressure which is mainly due to the change of the liquid phase entropy. Consequently, this evolution can be written:

$$T_m^0 = T_m^{0Patm} + 0.283 P - 2.08 \times 10^{-4} P^2 \quad (19)$$

In eq.18, the first term is the crystallization temperature at atmospheric pressure (126.1°C for a cooling rate of 2°C/min). This term is cooling rate dependent. In eq.19, the first term is the equilibrium melting temperature at atmospheric pressure which is the melting temperature of an hypothetical infinite crystal. There are different values for T_m^{0Patm} in the literature^{5,9,23,24} but it should be pointed out that it does not influence our further calculations. In this work, the value of 210°C was chosen⁵. Besides, Mezghani and Phillips⁹ reported the variation of T_m^0 with pressure for both α and γ phases of *i*-PP. Their results are close to eq.19, although they are shifted because of a different T_m^{0Patm} value (the derivatives are similar).

As a result, the Nakamura rate constant can be obtained for every pressure by a shift along the temperature scale given by the two last terms of eq.19. In other words, it means that when $K(T)$ is expressed versus the temperature, it obviously depends on the pressure but, when expressed versus

the supercooling, it becomes pressure independent as shown in Figure 6. Therefore the relative crystallinity can be calculated from eq.13 whatever the pressure.

Comparison with Experiments

At this stage, all the parameters in the heat equation (eq.1) were evaluated. So this equation can be resolved and the temperature and the specific volume for each time and each location in the sample can be obtained. Knowing this specific volume distribution for each time, an average specific volume, analogous to experimental data, can be deduced. This average specific volume is defined by the simple ratio between the sample volume and the sample weight:

$$\langle V_{sp} \rangle = \frac{\pi R^2 L}{L \int_0^R \frac{2\pi r dr}{V_{sp}(r)}} = \frac{R^2}{2 \int_0^R \frac{r dr}{V_{sp}(r)}} \quad (20)$$

The modeling of the specific volume was validated by calculating $\langle V_{sp} \rangle$ and comparing it to experimental results for different cooling rates (up to 35°C/min) and three pressures. For these calculations, the input final crystallinity values were measured on samples crystallized at atmospheric pressure with different cooling rates. These values are displayed in Table 2. Although there is not a great evolution of X_∞ with the cooling rate, the general trend is a decrease of X_∞ when the cooling rate increases. However, the slight effect of pressure on X_∞ (see Table 1) was not taken into account in the calculations.

Figure 7, 8 and 9 show the specific volume measured with cooling rates of 2, 10 and 35 °C/min respectively and for three pressures up to 100 MPa. As it can be seen in these Figures, the calculated average specific volumes $\langle V_{sp} \rangle$ are very close to the experimental points for all the cooling rates and pressures. Hence, it can be concluded that the modeling is quite suitable and, particularly, it correctly describes the pressure and the cooling rates effects on the crystallization.

Moreover, in these Figures, the intrinsic specific volume V_{sp}^{int} versus the control temperature is also plotted. Actually, this intrinsic specific volume stands for the result that would be obtained experimentally if there was no thermal gradient in the sample. Practically, it corresponds to the specific volume obtained at the sample periphery. Obviously, for a low cooling rate, the difference between the experimental and the intrinsic specific volumes is not significant (Figure 7). However, when the cooling rate increases, this difference becomes more and more important, especially, but not only, in the crystallization zone (Figures 8 and 9).

In Figure 10, the results are plotted for cooling rates of 2 and 35 °C/min and a pressure of 60 MPa. As it can be seen, in the liquid part, the rough experimental results are different from one cooling rate to the other, only because of the thermal gradient in the sample. Nevertheless, the intrinsic specific volume curves are obviously identical because the real specific volume in the liquid state is independent of the cooling rate. In the solid part of the diagram, the slight difference between the intrinsic curves is only due to a difference of final crystallinities caused by the different cooling rates. However, in the transition zone, experimental results show an important difference due not only to the thermal gradient but also to the effect of the cooling rate on the crystallization. As it can be noticed in Figure 10, the half of the difference between the two presented cooling rates arises from the crystallization kinetics which is revealed by the intrinsic specific volume curves. The other half of the difference is given by the thermal gradient. Therefore, both effects can be distinguished by the presented method.

The other output of the modeling is the temperature evolution inside the sample. As an example, Figure 11 shows the temperature in the sample axis and at the sample periphery versus time for three pressures and a cooling rate of 20°C/min. Outside the crystallization zone the temperature difference between the axis and the periphery is about 13°C. Compared to the solid state, the thermal gradient is slightly higher in the liquid state because the thermal conductivity is lower. Moreover, during the crystallization the temperature difference between the periphery and the axis can increase up to more than 30°C.

Furthermore, In Figure 12, the radial temperature distribution for different times is plotted showing a sliding regime before and after the crystallization (the lines are parallel). However, during the transition, the heat release leads to an alteration of this temperature profile.

CONCLUSION

In this study, it was shown that dilatometric measurements in isobaric cooling mode can be used to characterize the crystallization kinetics of polymers under pressure. Nevertheless, the rough experimental results must be analyzed by taking into account the thermal gradient in the sample. In our case, the specific volume of the purely amorphous phase was described using the Tait equation fitted on low cooling rate PVT experiments. The purely crystalline phase specific volume was considered linearly dependent on temperature and pressure. Then, the relative crystallinity was modeled by the Nakamura equation, suitable for non constant cooling rates. The rate constant of the Nakamura equation was obtained at atmospheric pressure from DSC experiments, with an Avrami exponent of 3. The pressure effect was drawn from the crystallization temperature pressure dependence which is directly linked to the equilibrium melting temperature variation with the pressure. Finally, the obtained intrinsic specific volume was validated by calculating the thermal gradient in the sample and comparing the average specific volume to the experimental one.

ACKNOWLEDGMENTS

The authors want to gratefully acknowledge the companies Legrand, Solvay and Moldflow for the material supply and characterization and for financial support.

REFERENCES:

- 1 Leute, U.; Dollhopf, W.; Liska, E. Dilatometric measurements on some polymers: the pressure dependence of thermal properties. *Colloid & Polymer Sci.* **1976**, *254* (3), 237-246.
- 2 He, J.; Zoller, P. Crystallization of Polypropylene, Nylon-66 and Poly(ethylene Terephthalate) at Pressures to 200 MPa: Kinetics and Characterization of Products. *J. of Polym. Sci: Part B: Polym. Phys.* **1994**, *32*, 1049-1067.
- 3 Hieber, C. A. Modelling the PVT Behavior of Isotactic Polypropylene. *Intern. Polymer Processing* **1997**, *XII* (3), 249-256.
- 4 Luyé, J. F.; Régnier, G.; Le Bot, P.; Delaunay, D.; Fulchiron, R. PVT Measurement Methodology for Semicrystalline Polymers to Simulate Injection Molding Process. *J. of Appl. Polym. Sci.* **2001**, *79* (2), 302-311.
- 5 Monasse, B.; Haudin, J. M. Growth transition and morphology change in polypropylene. *Colloid. Polym. Sci.* **1985**, *263*, 822-831.
- 6 Le Bot, P. *PhD Thesis*, ISITEM, University of Nantes , France **1998**.
- 7 Rodgers, P. A. Pressure-Volume-Temperature Relationships for Polymeric Liquids: A Review of Equations of State and Their Characteristic Parameters for 56 Polymers. *J. Appl. Polym. Sci.* **1993**, *48* (6), 1061-1080.
- 8 Wunderlich, B., in *Macromolecular Physics, Vol 1: Crystal Structure, Morphology, Defects*; Academic Press, New-York, 1973, 549 pp.
- 9 Mezghani, K.; Phillips, P. J. The γ -phase of high molecular weight isotactic polypropylene: III. The equilibrium melting point and the phase diagram. *Polymer* **1998**, *39* (16), 3735-3744.
- 10 Nakamura, K.; Watanabe, T.; Katayama, K.; Amono, T. Some Aspects of Nonisothermal Crystallization of Polymers. I. Relationship Between Crystallization Temperature, Crystallinity, and Cooling Conditions. *J. Appl. Polym. Sci.* **1972**, *16*, 1077-1091.

- 11 Nakamura, K.; Katayama, K.; Amono, T. Some Aspects of Nonisothermal Crystallization of Polymers. II. Consideration of the Isokinetic Condition. *J. Appl. Polym. Sci.* **1973**, *17*, 1031-1041.
- 12 Avrami, M. Kinetics of Phase Change. I General Theory. *J. Chem. Phys.* **1939**, *7*, 1103-1112.
- 13 Avrami, M. Kinetics of Phase Change. II Transformation-Time Relations for Random Distribution of Nuclei. *J. Chem. Phys.* **1940**, *8*, 212-224.
- 14 Avrami, M. Kinetics of Phase Change. III Granulation, Phase Change, and Microstructure. *J. Chem. Phys.* **1941**, *9*, 177-184.
- 15 Ozawa, T. Kinetics of non-isothermal crystallization. *Polymer* **1971**, *12* (3), 150-158.
- 16 Hieber, C. A. Correlations for the quiescent crystallization kinetics of isotactic polypropylene and poly(ethyleneterephthalate). *Polymer* **1995**, *36* (7), 1455-1467.
- 17 Di Lorenzo, M. L.; Silvestre, C. Non-isothermal crystallization of polymers. *Prog. Polym. Sci.* **1999**, *24*, 917-950.
- 18 Monasse, B.; Haudin, J. M. Thermal dependence of nucleation and growth rate in polypropylene by non isothermal calorimetry. *Colloid Polym. Sci.* **1986**, *264*, 117-122.
- 19 Eder, M.; Wlochowicz A. Kinetics of non-isothermal crystallization of polyethylene and polypropylene. *Polymer* **1983**, *24* (12), 1593-1595.
- 20 Hammami, A.; Spruiell, J. E.; Mehrotra, A. K. Quiescent nonisothermal crystallization kinetics of isotactic polypropylenes. *Polym. Eng. Sci.* **1995**, *35* (10), 797-804.
- 21 Angeloz, C.; Fulchiron, R.; Douillard, A.; Chabert, B.; Fillit, R.; Vautrin, A.; David, L. Crystallization of isotactic polypropylene under high pressure (γ phase). *Macromolecules* **2000**, *33* (11), 4138-4145.
- 22 Won, J. C.; Fulchiron, R.; Douillard, A.; Chabert, B.; Varlet, J.; Chomier, D. The crystallization kinetics of polyamide 66 in non-isothermal and isothermal conditions : effect of nucleating agent and pressure. *Polym. Eng. Sci.*, **2000**, *40* (9), 2058-2071.

- 23 Cheng, S. Z. D.; Janimak, J. J.; Zhang, A.; Cheng, H. N. Regime Transitions in Fractions of Isotactic Polypropylene. *Macromolecules* **1990**, *23* (1), 298-303.
- 24 Kim, Y. C., Kim, C. Y., Kim, S. C. Crystallization Characteristics of Isotactic Polypropylene With and Without Nucleating Agents. *Polym. Eng. Sci.* **1991**, *31* (14), 1009-1014.

TABLE 1:

Evolution of the crystallinity with the crystallization pressure (Cooling rate: 1°C/min).

Pressure (MPa)	0.1	20	60	100
X_{∞}	0.677	0.663	0.634	0.623

TABLE 2:

Evolution of the crystallinity with the cooling rate (samples crystallized at atmospheric pressure)

Cooling rate (°C/min)	1	2	5	10	20	30	35	40
X_{∞}	0.677	0.669	0.597	0.582	0.587	0.545	0.602	0.568

FIGURE CAPTIONS:

Figure 1:

PVT diagram of *i*-PP obtained in isobaric mode with a cooling rate of 1°C/min. Symbols are experimental data. Solid lines are calculated using eq.9, eq.10 and eq.11. The arrow indicates the specific volume of the amorphous phase at ambient pressure and temperature given in Ref 8.

Figure 2:

Solid part of the PVT diagram of *i*-PP obtained in isobaric mode with a cooling rate of 1°C/min. Symbols: Experimental data. Dashed lines: eq.8 with $\alpha=1$, $X_\infty=0.684$ and constant V_c . Solid lines: eq.8 with $\alpha=1$, $X_\infty=0.684$ and V_c given by eq.12.

Figure 3:

Nakamura rate constant obtained at atmospheric pressure from isothermal and constant cooling rate DSC experiments. Solid line given by eq.17.

Figure 4:

Relative crystallinity obtained at constant cooling rate and atmospheric pressure. Experimental data and Nakamura equation.

Figure 5:

Temperature of the crystallization onset (T_c) versus the pressure for a cooling rate of 2°C/min. Symbols: experimental points. Solid line: eq.18 with $T_c^{Patm} = 126.1^\circ\text{C}$.

Figure 6:

Nakamura rate constant $K(T)$: a) versus Temperature, b) versus supercooling.

Figure 7:

Specific Volume of *i*-PP versus control temperature for a cooling rate of 2°C/min.

Symbols: Experimental data, $\langle V_{sp} \rangle$ given by eq.20, V_{sp}^{int} : Intrinsic specific volume.

Figure 8:

Specific Volume of *i*-PP versus control temperature for a cooling rate of 10°C/min.

Symbols: Experimental data, $\langle V_{sp} \rangle$ given by eq.20, V_{sp}^{int} : Intrinsic specific volume.

Figure 9:

Specific Volume of *i*-PP versus control temperature for a cooling rate of 35°C/min.

Symbols: Experimental data, $\langle V_{sp} \rangle$ given by eq.20, V_{sp}^{int} : Intrinsic specific volume.

Figure 10:

Specific Volume of *i*-PP versus control temperature for two cooling rates and a pressure of 60 MPa.

Symbols: Experimental data, $\langle V_{sp} \rangle$ given by eq.20, V_{sp}^{int} : Intrinsic specific volume.

Figure 11:

Temperature evolution in the PVT sample for a cooling rate of 20°C/min and 3 pressures.

Figure 12:

Temperature profile in the PVT sample (cooling rate: 20°C/min, Pressure: 60 MPa) at different times.

Figure 1

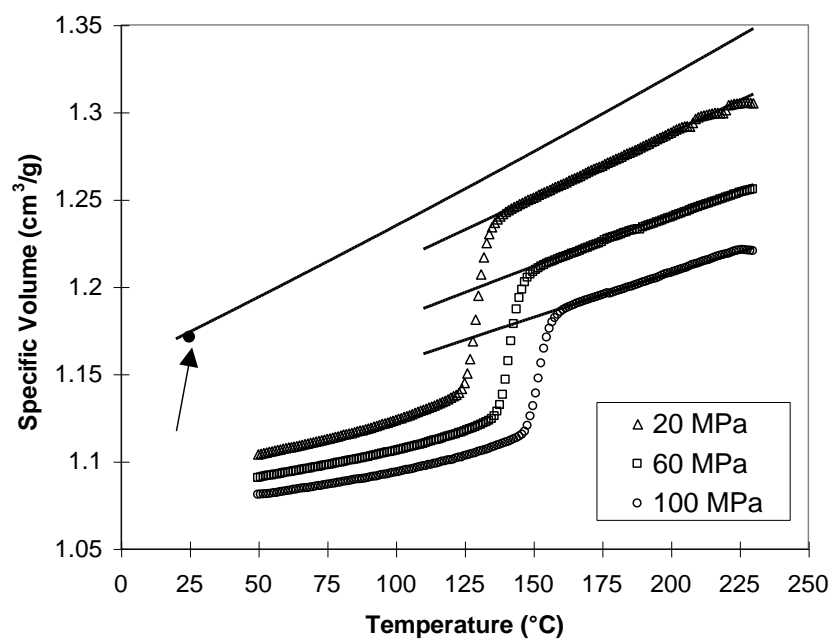


Figure 2

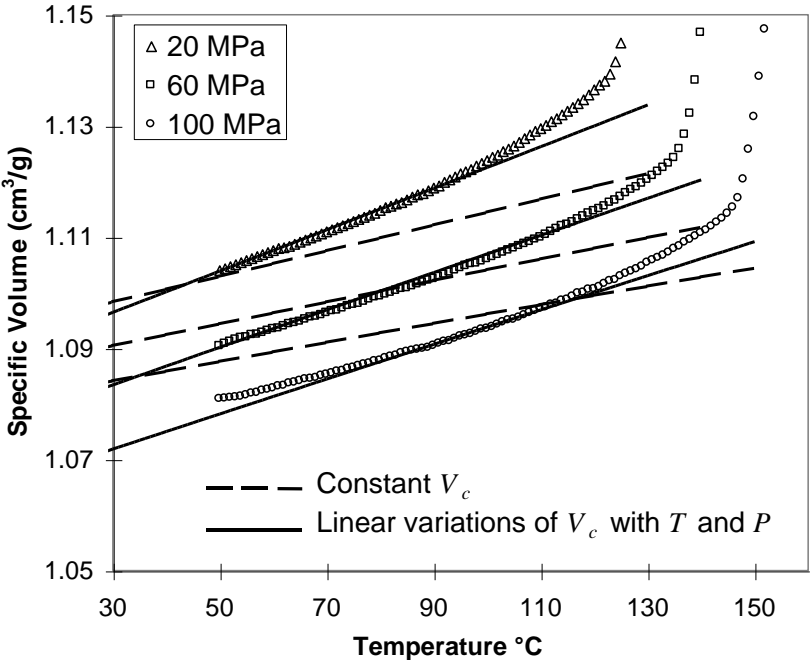


Figure 3

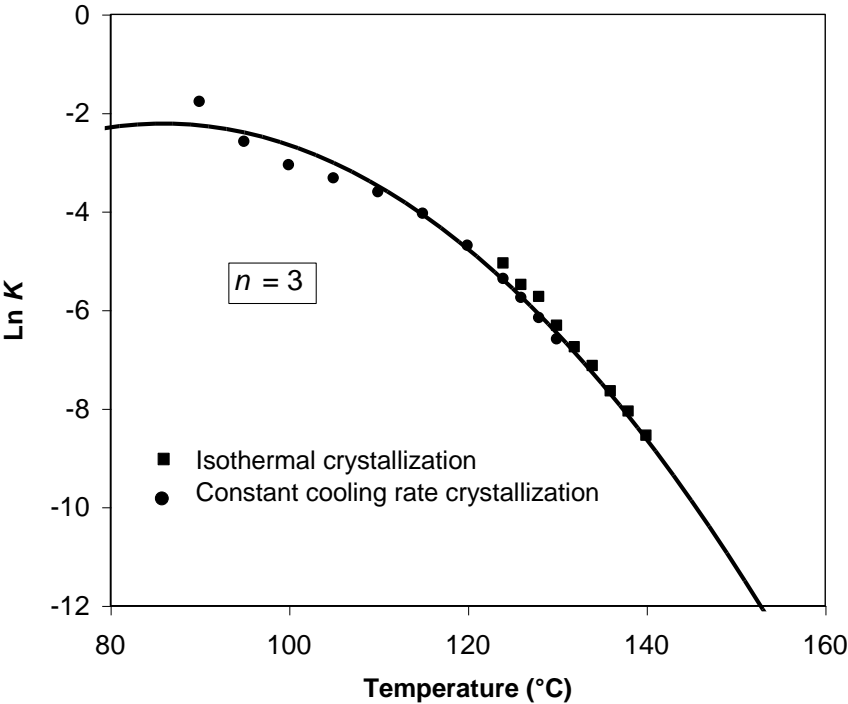


Figure 4

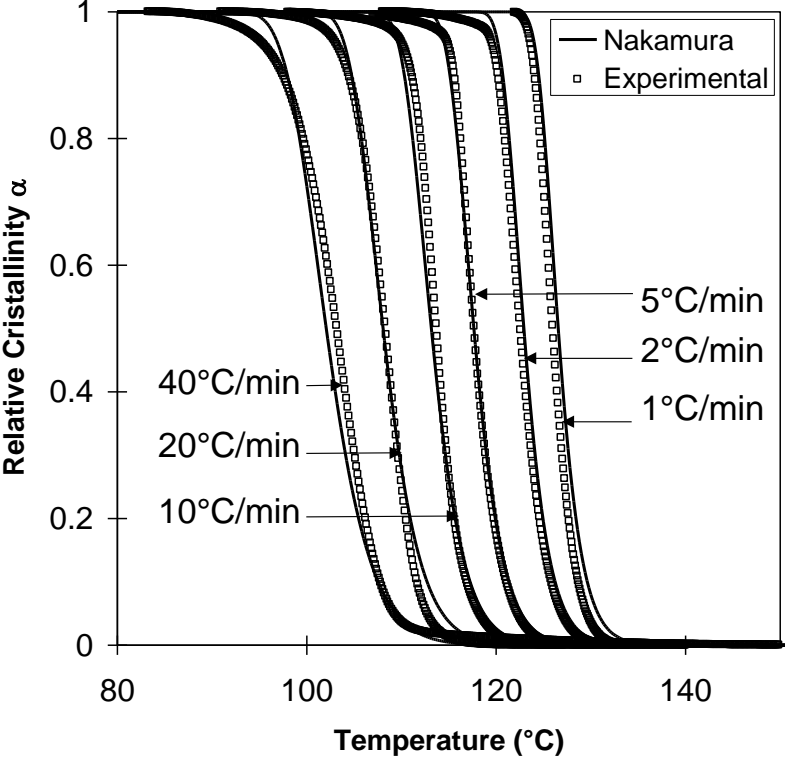


Figure 5

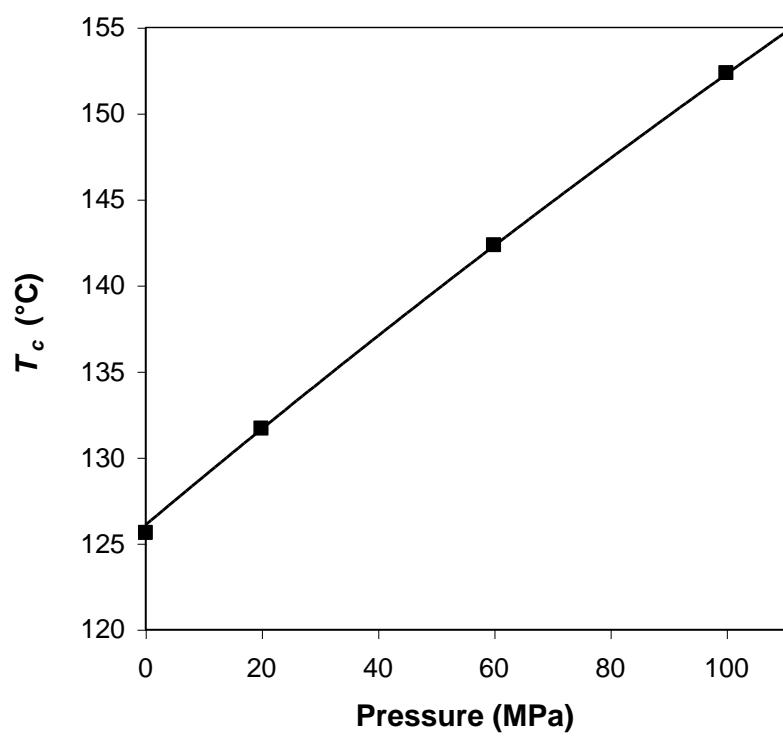


Figure 6

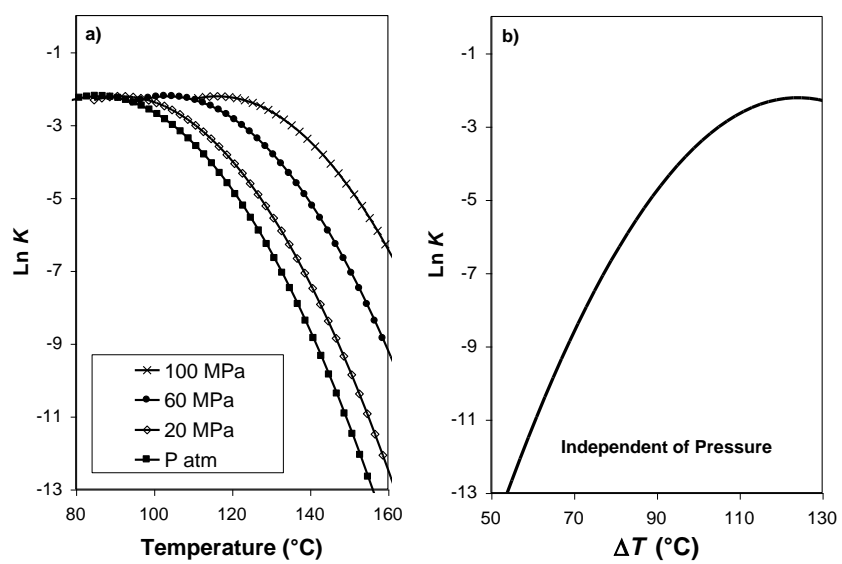


Figure 7:

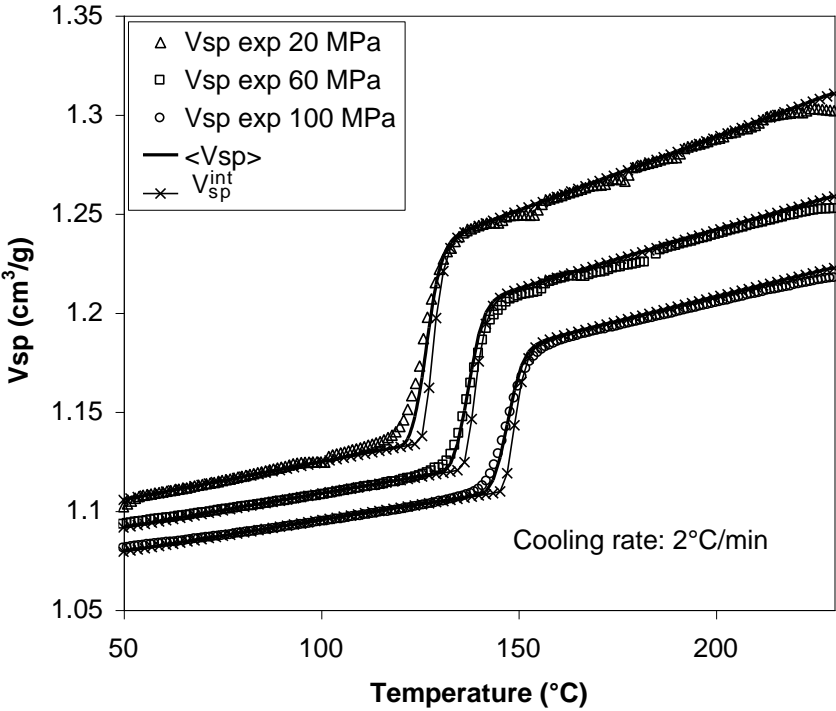


Figure 8:

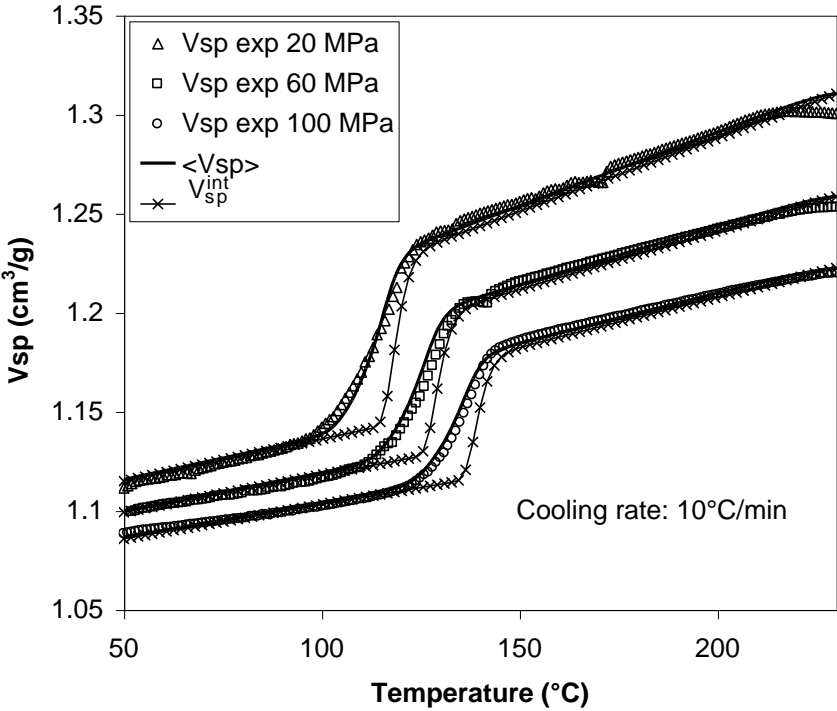


Figure 9:

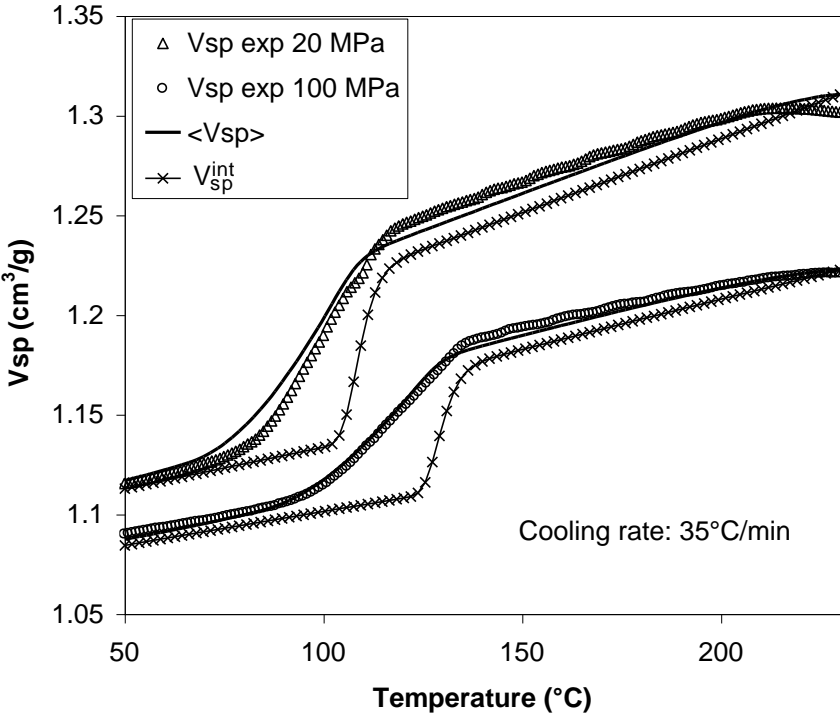


Figure 10:

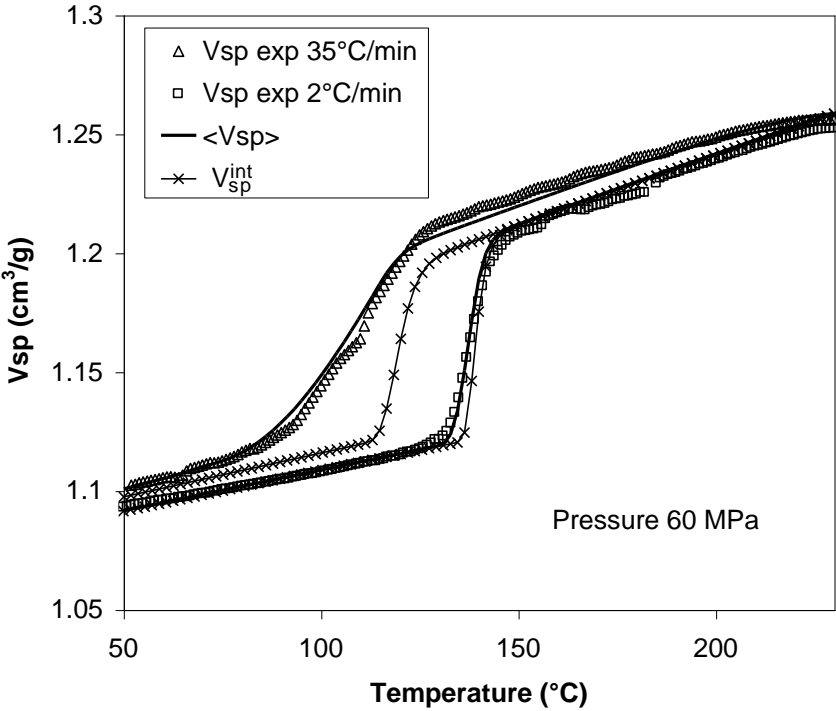


Figure 11:

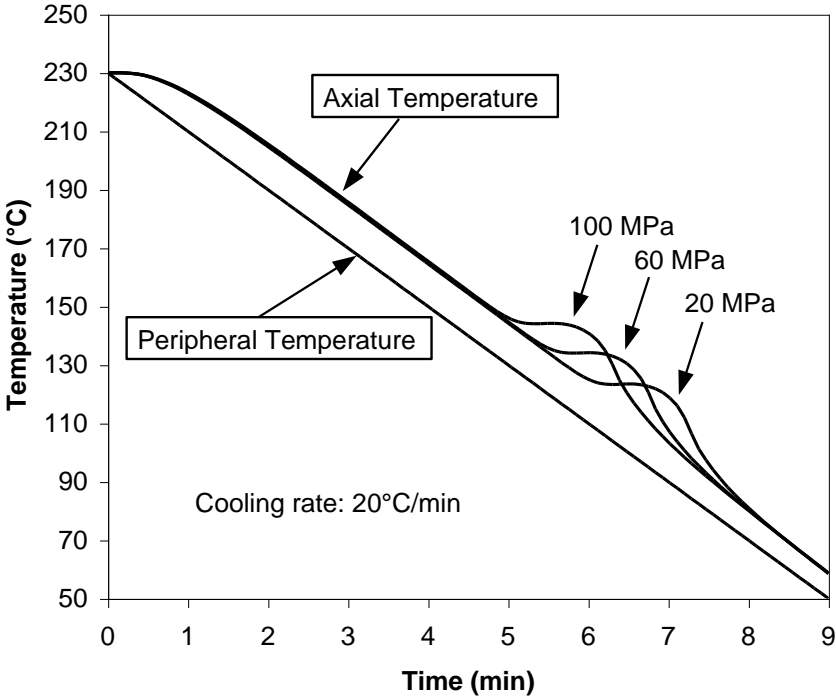


Figure 12:

